Cross sections of neutron-induced reactions

Tapan Mukhopadhyay,* Joydev Lahiri,† and D. N. Basu‡
Variable Energy Cyclotron Centre, 1/AF Bidhan Nagar, Kolkata 700064, India
(Received 14 June 2010; revised manuscript received 19 August 2010; published 26 October 2010)

We study the properties of the neutron-nucleus total and reaction cross sections for several nuclei. We have applied an analytical model, the nuclear Ramsauer model, justified it from the nuclear reaction theory approach, and extracted the values of 12 parameters used in the model. The given parametrization has an advantage as phenomenological optical model potentials are limited up to 150–200 MeV. The present model provides good estimates of the total cross sections for several nuclei particularly at high energies.

DOI: 10.1103/PhysRevC.82.044613 PACS number(s): 24.10.−i, 25.40.−h, 25.60.Dz, 28.20.Cz

I. INTRODUCTION

Recently, the accelerator-driven subcritical systems (ADSS) and their neutronics have been studied by many researchers [1–6]. The subcritical reactor is driven critically by spallation neutrons produced by bombarding a high-energy proton beam with high current (greater than ∼10 mA) [7] on a heavy element target. Such a system serves a dual purpose of energy multiplication and waste incineration of the long-lived radioactive waste produced in reactors based on thermal neutron-induced fission. Reactor physics calculations of ADSS require neutron-nucleus scattering cross sections up to 500-MeV neutron energies. Unlike the thermal neutron-induced fission, the energy spectrum of spallation neutrons can reach up to several hundred MeV. In this context it is important to study the systematics of neutron absorption and scattering cross sections on various nuclei for neutron energies up to several hundred MeV.

Recently the scaling properties of proton-nucleus total reaction cross sections for stable nuclei of the whole mass-number region have been studied [8] and found to be in proportion to $\propto Z^{2/3}\sigma_{pp}^{\text{total}} + N^{2/3}\sigma_{pn}^{\text{total}}$ within 10% uncertainty. This parametrization can be understood considering the target nucleus as constituted of proton and neutron fluids and cross sections, in a geometric model, proportional to the square of their radii which in turn are proportional to $\sigma_{pp}^{\text{total}} Z^{2/3}$ and $\sigma_{pn}^{\text{total}} N^{2/3}$ respectively. However, we find that the apparently obvious extension of this approximate expression for proton-nucleus reaction cross section to neutron-nucleus (n-N) reaction cross section as $\propto Z^{2/3}\sigma_{pn}^{\text{total}} + N^{2/3}\sigma_{nn}^{\text{total}}$ does not lead to any reasonably acceptable results. In this work, therefore, we propose an analytical approach based on the nuclear Ramsauer model to successfully estimate the energy dependence of total cross section (σ_{tot}), the scattering cross section (σ_{sc}), and the reaction cross section (σ_r) for the n-N interaction and predict these cross sections for actinides.

II. THE ANALYTICAL MODEL

The basic picture of the analytical model is that the forward-scattering amplitude for a neutron incident on a nucleus represented by a potential well of radius R is given by nuclear reaction theory as follows:

$$f(0^o) = \frac{i}{2k}\sum_{l=0}^{L}(2l+1)(1-e^{2i\delta_l}), \tag{1}$$

where the complex phase shift δ_l may be considered as independent of angular momenta l of the l-th partial wave [9]. The above expression after summing over l then reduces to

$$f(0^o) = ik(R+\lambda\!\!\!^{-})^2(1-\alpha e^{i\beta})/2, \tag{2}$$

where $e^{2i\delta_l}$ is replaced by $\alpha e^{i\beta}$, with β being 2 times the real part of the phase shift and α arising out of imaginary part of the phase shift (which takes care of the attenuation or loss of flux). In this analytical model, the cutoff, that is, the maximum value L of l, is taken as kR.

In this approach since the total cross section is related to the imaginary part of the forward scattering amplitude by $\sigma_{\text{tot}} = \frac{4\pi}{k} Imf(0^o)$, the total cross section (σ_{tot}), the scattering cross section (σ_{sc}), and the reaction cross section (σ_r) are given by:

$$\begin{aligned}\sigma_{\text{tot}} &= 2\pi(R+\lambda\!\!\!^{-})^2(1-\alpha\cos\beta),\\ \sigma_{\text{sc}} &= \pi(R+\lambda\!\!\!^{-})^2(1+\alpha^2-2\alpha\cos\beta),\\ \sigma_r &= \pi(R+\lambda\!\!\!^{-})^2(1-\alpha^2),\\ \text{where}\quad \lambda\!\!\!^{-} &= \hbar/\sqrt{2mE}\end{aligned} \tag{3}$$

and E is the incident neutron energy in the center-of-mass system, m is the neutron mass, and $-V - iW$ is the nuclear n-N interaction potential with V and W as positive quantities and contains no Coulomb interaction. The phase shift δ in a WKB approximation is $[\int K'dr - \int k'dr]$ and the real part of it to a zeroth-order approximation [10] for a square well with radius R is $(K-k)R$, where K and k are the real parts of K' and k', respectively. The real wave numbers inside and outside the nucleus are, therefore, given by $K^2 = 2m(E+V)/\hbar^2$ and $k^2 = 2mE/\hbar^2$, respectively. Hence β is determined by the real potential V,

$$\beta = 2(K-k)R = 2\frac{(2m)^{\frac{1}{2}}}{\hbar}[\sqrt{E+V}-\sqrt{E}]R, \tag{4}$$

whereas the attenuation factor α is determined primarily by the imaginary potential W,

$$\alpha = e^{-\bar{R}/\Lambda} = e^{-2mW\bar{R}/\hbar^2 K}, \tag{5}$$

*tkm@veccal.ernet.in
†joy@veccal.ernet.in
‡dnb@veccal.ernet.in

TABLE I. The parameter values extracted using the experimental data with errors for total neutron cross sections of nuclei ^{238}U and ^{184}W and their weighted averages. The weighted averaged parameter values are used in the subsequent calculations.

Parameter	Using ^{238}U data	Using ^{184}W data	Weighted average
V_0	45.89 ± 0.04	44.18 ± 0.22	45.64 ± 0.07
V_1	6.72 ± 0.06	7.37 ± 0.57	6.82 ± 0.13
V_2	-118.18 ± 3.24	-117.65 ± 20.49	-118.10 ± 5.75
V_E	-3.18 ± 0.01	-3.05 ± 0.02	-3.16 ± 0.01
α_0	$(28.67 \pm 0.82) \times 10^{-3}$	$(29.77 \pm 4.33) \times 10^{-3}$	$(28.83 \pm 1.33) \times 10^{-3}$
α_1	$(-2.84 \pm 0.01) \times 10^{-3}$	$(-2.84 \pm 0.10) \times 10^{-3}$	$(-2.84 \pm 0.03) \times 10^{-3}$
α_2	$(13.21 \pm 0.01) \times 10^{-2}$	$(14.21 \pm 0.12) \times 10^{-2}$	$(13.35 \pm 0.03) \times 10^{-2}$
r_1	$1.37423 \pm 0.27 \times 10^{-3}$	$1.39555 \pm 0.88 \times 10^{-3}$	$1.37655 \pm 0.34 \times 10^{-3}$
γ	$(7.93 \pm 0.04) \times 10^{-3}$	$(7.93 \pm 0.12) \times 10^{-3}$	$(7.93 \pm 0.05) \times 10^{-3}$
r_{10}	$(-23.23 \pm 0.03) \times 10^{-3}$	$(-20.01 \pm 0.25) \times 10^{-3}$	$(-22.76 \pm 0.06) \times 10^{-3}$
r_{11}	$(112.95 \pm 0.26) \times 10^{-3}$	$(92.41 \pm 2.95) \times 10^{-3}$	$(109.95 \pm 0.65) \times 10^{-3}$
r_2	$(25.54 \pm 0.20) \times 10^{-2}$	$(13.00 \pm 1.26) \times 10^{-2}$	$(23.71 \pm 0.35) \times 10^{-2}$

where Λ is the mean free path of the neutron inside the nucleus and the average chord length of a neutron passing through the nucleus is $\bar{R} = \frac{4}{3}R$ [11,12]. Since $R \propto A^{\frac{1}{3}}$ ($R \sim r_0 A^{\frac{1}{3}}$), the above arguments imply that $\beta = \beta_0 A^{\frac{1}{3}}[\sqrt{E+V} - \sqrt{E}]$, where $\beta_0 = \frac{2r_0(2m)^{\frac{1}{2}}}{\hbar}$ whose value is approximately 0.6. The nuclear radius parameter r_0 is fitted to $r_1 A^{\gamma}$. The attenuation factor, which is much less than unity but increases with energy (obvious from its expression above), can be written as $\alpha = \alpha_0 + \alpha_A\sqrt{E}$ and is assumed to be weakly mass dependent [13] as $\alpha_A = \alpha_1 \ln A + \alpha_2/\ln A$ due to the imaginary potential. The first term $V_A = V_0 + V_1(1 - 2Z/A) + V_2/A$ of the real potential $V = V_A + V_E\sqrt{E}$ contains both the isoscalar and the isovector [14,15] components of the optical model potential (OMP) where Z is the atomic number of the target nucleus, whereas the second term accounts for its energy dependence.

III. EVALUATION OF THE ANALYTICAL MODEL

The Ramsauer model can be fitted to the experimental neutron total cross sections using Eq. (3). The nuclear radius R can be parametrized as $R = r_0 A^{\frac{1}{3}} + r_A\sqrt{E} + r_2$ with $r_A = r_{10}\ln A + r_{11}/\ln A$. As mentioned above, the value of β_0 is fixed at 0.5928. For evaluation of other parameters, the measured neutron total cross sections for nuclei ^{238}U and ^{184}W along with respective experimental errors are used for fitting to extract two sets of values. The final set of parameters is extracted from the weighted average of these two sets defining $w_1 = \frac{n_1}{n_1+n_2}$ and $w_2 = \frac{n_2}{n_1+n_2}$ as weight factors for ^{238}U and ^{184}W, respectively, where n_1 and n_2 are the corresponding number of data points used for these two nuclei. The parameter values obtained from the data of these two nuclei and their weighted average are provided in Table I.

IV. CALCULATION AND RESULTS

Each calculation is performed at neutron incident energy intervals of 1 MeV and for various elements. Table II, contains the results of the calculations for the total and reaction cross sections for neutrons on ^{208}Pb at few energies which are compared with those obtained using the Wicks limit [16] approach, Koning-Delaroche global OMP, Morillon-Romain global OMP, and Koning-Delaroche lead OMP [17]. The deviation for the 7-MeV result is a consequence of the fact that the Ramsauer model is less reliable for neutron energies below 10 MeV [18]. Nevertheless, the Ramsauer model has an advantage as the phenomenological OMPs are limited up to 150–200 MeV; however, they are expected to be more accurate in that energy range. In Figs. 1–9, the variations of the total cross section ($\sigma_{\rm tot}$), the scattering cross section ($\sigma_{\rm sc}$), and the reaction cross section (σ_r) with incident neutron energy are plotted for ^{238}U, ^{232}Th, ^{209}Bi, ^{208}Pb, ^{197}Au, ^{182}W, ^{184}W, ^{186}W, and ^{181}Ta target nuclei. The continuous lines represent the total cross sections, the dashed lines represent the scattering cross sections, and the dotted lines represent the reaction cross sections while the hollow circles represent the experimental data [19–21] for $\sigma_{\rm tot}$ which show reasonable agreement. In Fig. 10 estimates of these cross sections are plotted for the ^{239}Pu target.

TABLE II. Total and reaction cross sections for neutrons on ^{208}Pb for the (a) present calculations and those obtained using (b) Wicks limit [16], (c) Koning-Delaroche global OMP, (d) Morillon-Romain global OMP, and (e) Koning-Delaroche lead OMP [17].

$E_n^{\rm lab}$ (MeV)	(a)$\sigma_{\rm tot}$ (barns)	(b)$\sigma_{\rm tot}$ (barns)	(c)$\sigma_{\rm tot}$ (barns)	(d)$\sigma_{\rm tot}$ (barns)	(e)$\sigma_{\rm tot}$ (barns)	(a)σ_r (barns)	(b)σ_r (barns)	(c)σ_r (barns)	(d)σ_r (barns)	(e)σ_r (barns)
7	6.617	5.78	5.813	5.790	6.035	3.264	2.393 ± 0.045	3.309	3.236	3.641
14	5.635	–	5.289	5.406	5.230	2.878	–	2.763	2.841	2.686
20	5.834	5.85	5.793	5.770	5.783	2.714	2.477 ± 0.046	3.315	3.277	3.271
22	5.774	5.79	5.792	5.716	5.835	2.672	2.538 ± 0.044	3.309	3.230	3.309
24	5.651	5.67	5.708	5.609	5.780	2.636	2.450 ± 0.044	3.222	3.122	3.256

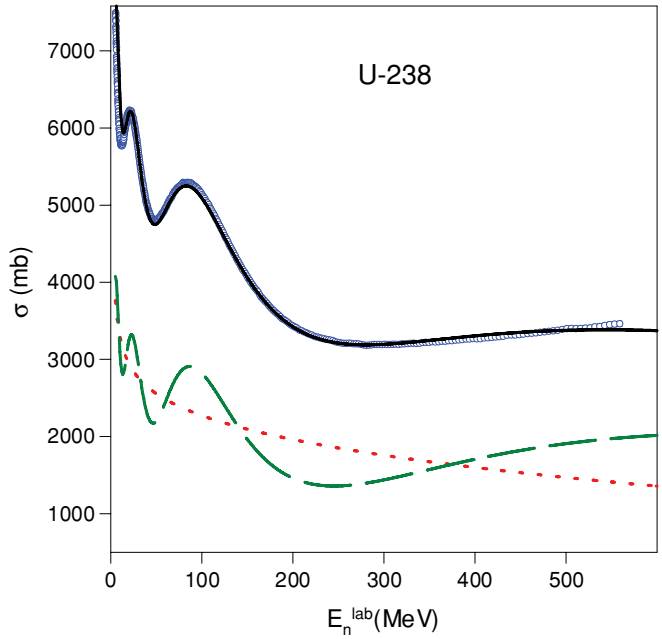

FIG. 1. (Color online) The plots of total cross section ($\sigma_{\rm tot}$), the scattering cross section ($\sigma_{\rm sc}$), and the reaction cross section (σ_r) versus incident neutron energy for ^{238}U target. The continuous line represents the total cross section, the dashed line represents the scattering cross section, the dotted line represents the reaction cross section, and the open circles represent the experimental data.

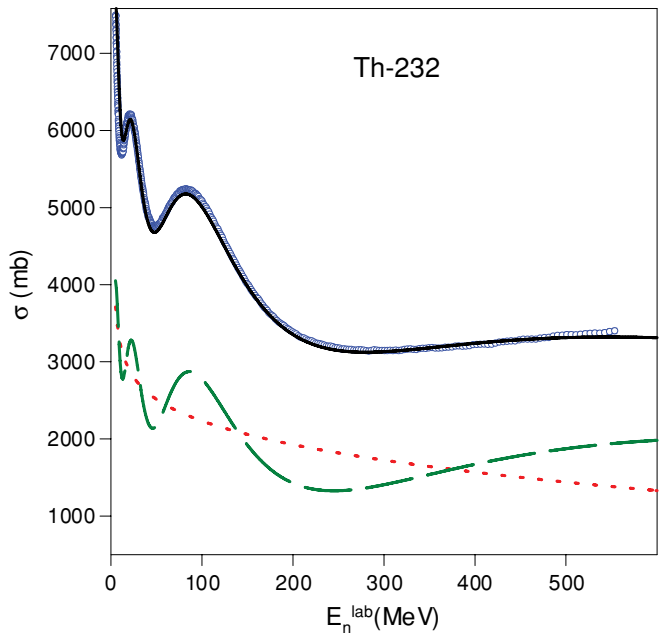

FIG. 2. (Color online) The plots of total cross section ($\sigma_{\rm tot}$), the scattering cross section ($\sigma_{\rm sc}$), and the reaction cross section (σ_r) versus incident neutron energy for ^{232}Th target. The continuous line represents the total cross section, the dashed line represents the scattering cross section, the dotted line represents the reaction cross section, and the open circles represent the experimental data.

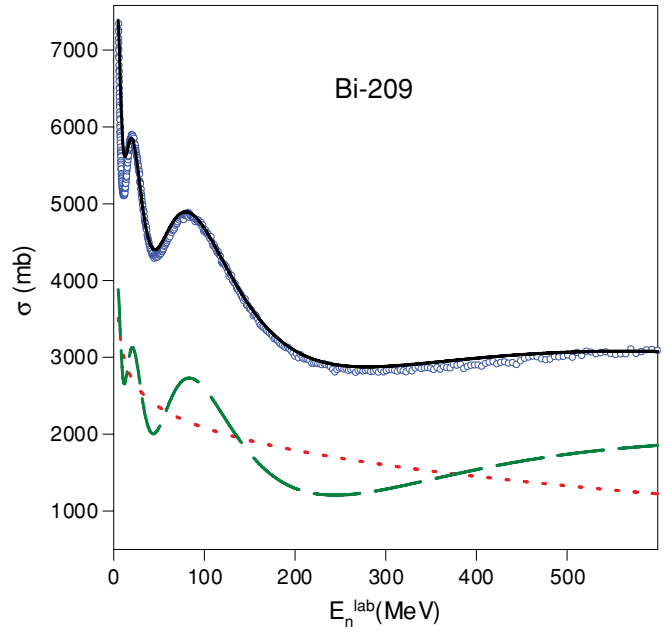

FIG. 3. (Color online) The plots of total cross section ($\sigma_{\rm tot}$), the scattering cross section ($\sigma_{\rm sc}$), and the reaction cross section (σ_r) versus incident neutron energy for ^{209}Bi target. The continuous line represents the total cross section, the dashed line represents the scattering cross section, the dotted line represents the reaction cross section, and the open circles represent the experimental data.

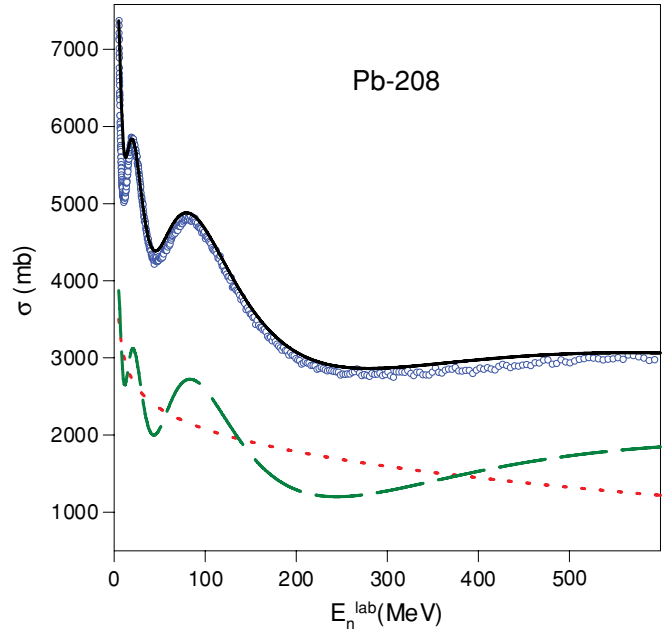

FIG. 4. (Color online) The plots of total cross section ($\sigma_{\rm tot}$), the scattering cross section ($\sigma_{\rm sc}$), and the reaction cross section (σ_r) versus incident neutron energy for ^{208}Pb target. The continuous line represents the total cross section, the dashed line represents the scattering cross section, the dotted line represents the reaction cross section, and the open circles represent the experimental data.

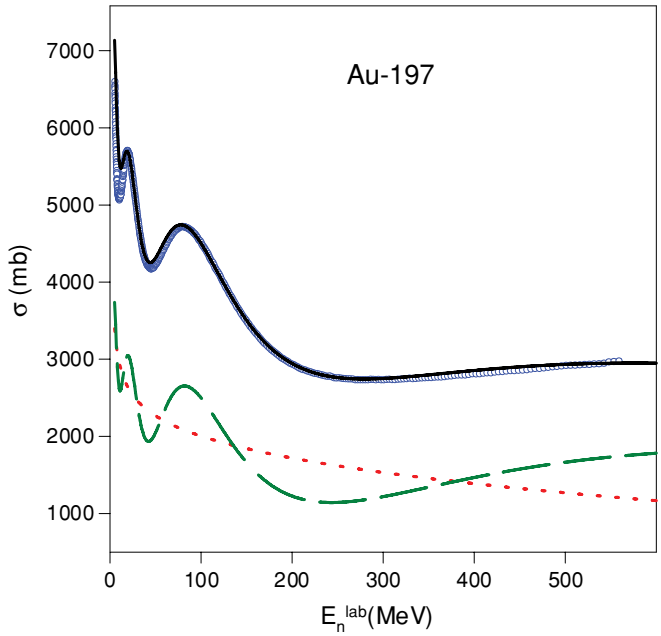

FIG. 5. (Color online) The plots of total cross section (σ_{tot}), the scattering cross section (σ_{sc}), and the reaction cross section (σ_r) versus incident neutron energy for ^{197}Au target. The continuous line represents the total cross section, the dashed line represents the scattering cross section, the dotted line represents the reaction cross section, and the open circles represent the experimental data.

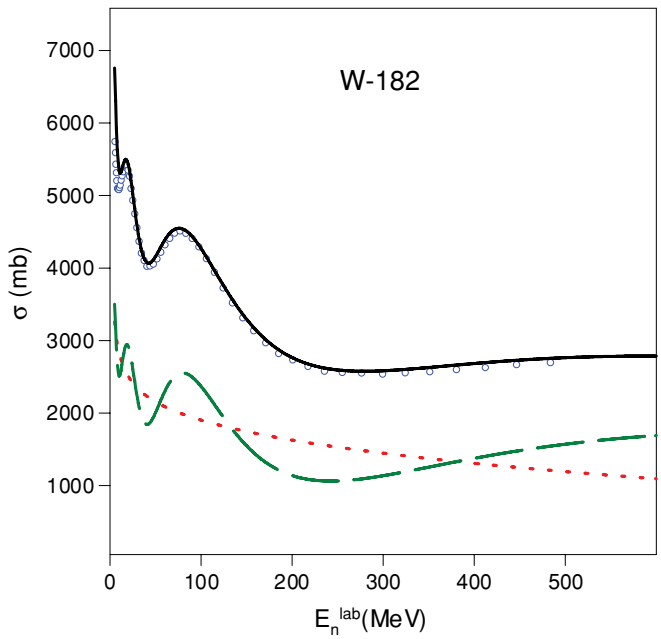

FIG. 6. (Color online) The plots of total cross section (σ_{tot}), the scattering cross section (σ_{sc}), and the reaction cross section (σ_r) versus incident neutron energy for ^{182}W target. The continuous line represents the total cross section, the dashed line represents the scattering cross section, the dotted line represents the reaction cross section, and the open circles represent the experimental data.

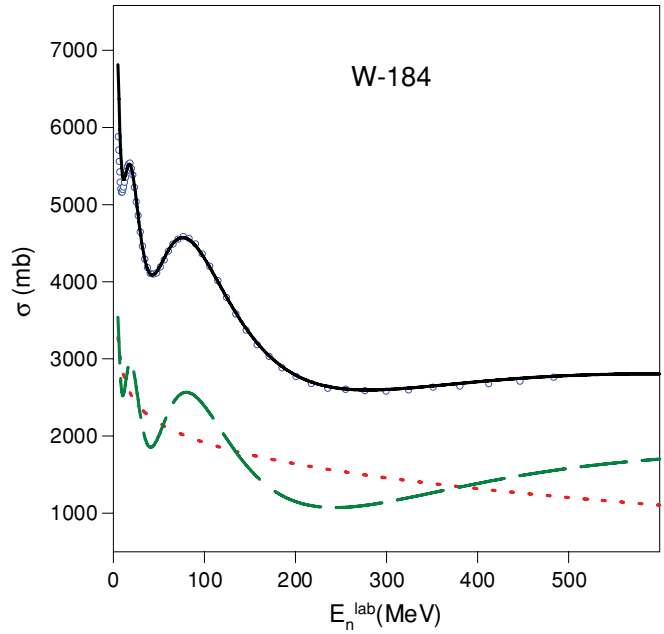

FIG. 7. (Color online) The plots of total cross section (σ_{tot}), the scattering cross section (σ_{sc}), and the reaction cross section (σ_r) versus incident neutron energy for ^{184}W target. The continuous line represents the total cross section, the dashed line represents the scattering cross section, the dotted line represents the reaction cross section, and the hollow circles represent the experimental data.

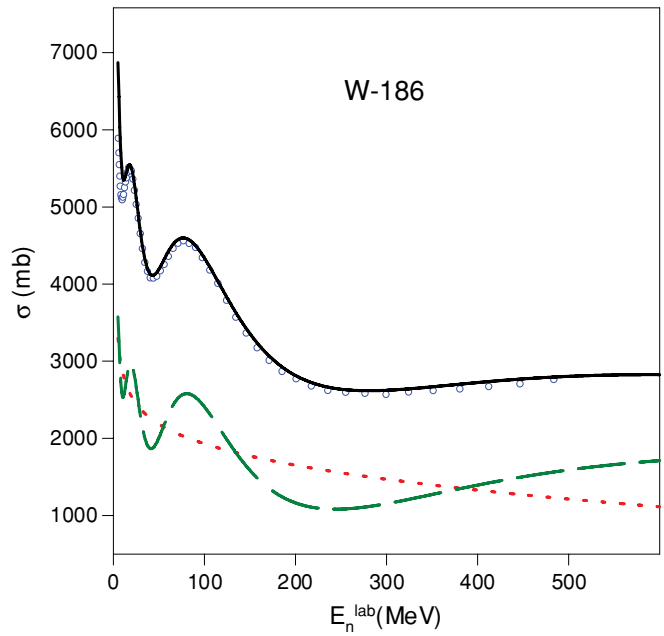

FIG. 8. (Color online) The plots of total cross section (σ_{tot}), the scattering cross section (σ_{sc}), and the reaction cross section (σ_r) versus incident neutron energy for ^{186}W target. The continuous line represents the total cross section, the dashed line represents the scattering cross section, the dotted line represents the reaction cross section, and the open circles represent the experimental data.

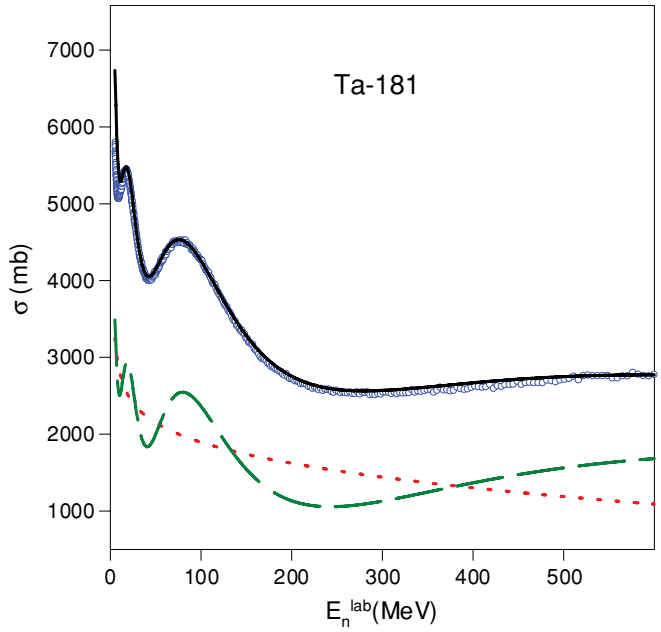

FIG. 9. (Color online) The plots of total cross section (σ_{tot}), the scattering cross section (σ_{sc}), and the reaction cross section (σ_r) versus incident neutron energy for ^{181}Ta target. The continuous line represents the total cross section, the dashed line represents the scattering cross section, the dotted line represents the reaction cross section, and the open circles represent the experimental data.

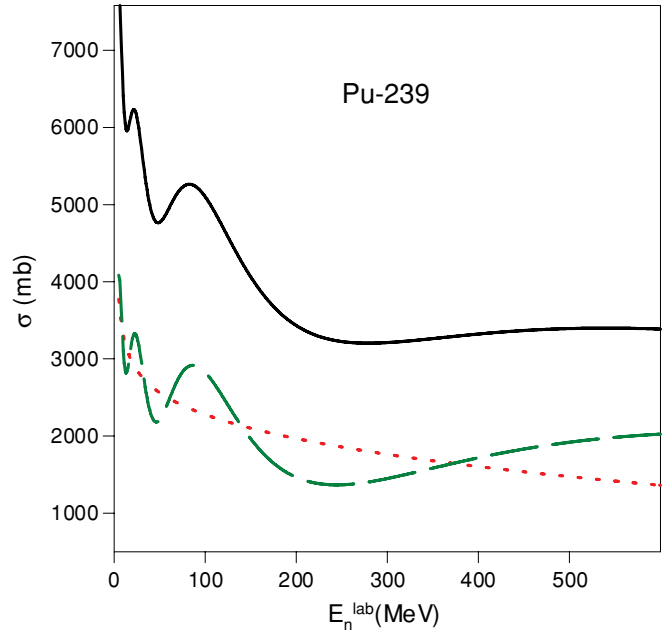

FIG. 10. (Color online) The plots of total cross section (σ_{tot}), the scattering cross section (σ_{sc}), and the reaction cross section (σ_r) versus incident neutron energy for ^{239}Pu target. The continuous line represents the total cross section, the dashed line represents the scattering cross section and the dotted line represents the reaction cross section.

V. SUMMARY AND CONCLUSION

In summary, we find that the apparently obvious extension of a moderately successful approximate expression for proton-nucleus reaction cross section to the neutron-nucleus reaction cross section does not lead to any reasonably acceptable results. We have applied an analytical model, the nuclear Ramsauer model, justified it from the optical model and nuclear reaction theory approach, derived the systematics and performed calculations of neutron-nucleus total cross section (σ_{tot}), the scattering cross section (σ_{sc}), and the reaction cross section (σ_r) for various elements and compared with measured total cros sections. We have also predicted these cross sections for ^{239}Pu. It is observed that the Ramsauer model fits are sensitive to nuclear radius parameter and by fine adjustment of this parameter one can obtain very good global fits for various systems to the neutron total cross sections. The given parametrization has an advantage as phenomenological optical model potentials are limited up to 150–200 MeV; however, they are expected to be more accurate in that energy range. We conclude that these neutron-nucleus reaction cross sections are very useful for the theoretical calculations of radioactive ion beam [22,23] production. These can also be used for performing Hauser-Feshbach [24] calculations with Monte Carlo simulations [25] to estimate the cross sections for neutron induced fission [26], evaporation residues, or evaporation neutron multiplicities [27] and for comparison of the photon [26,27] versus nucleon induced fission as well. Moreover, the neutron-scattering cross sections are very important for reactor physics calculations [1–7] of the ADSS applications.

[1] A. Boudard *et al.*, Nucl. Phys. A **663**, 1061c (2000).
[2] C. H. M. Broeders and I. Broeders, Nucl. Eng. Des. **202**, 209 (2000).
[3] I. Demirkol *et al.*, Nucl. Sci. Eng. **147**, 83 (2004).
[4] I. Demirkol *et al.*, Chin. J. Phys. **46**, 124 (2008).
[5] A. Kaplan *et al.*, Appl. Radiat. Isotopes **67**, 570 (2009).
[6] H. Yapc *et al.*, Ann. Nucl. Energy **34**, 374 (2007).
[7] C. Rubbia *et al.*, Conceptual design of a fast Neutron Operated High power Energy Amplifier, CERN Rep, CERN/AT/95-44 (ET), Geneva, September 29,1995.
[8] Badawy Abu-Ibrahim and Akihisa Kohama, Phys. Rev. C **81**, 057601 (2010).
[9] J. D. Lawson, Philos. Mag. **44**, 102 (1953).
[10] C. B. O. Mohr, Aust. J. Phys. **10**, 110 (1957).
[11] C. R. Gould, D. G. Haase, L. W. Seagondollar, J. P. Soderstrum, K. E. Nash, M. B. Schneider, and N. R. Roberson, Phys. Rev. Lett. **57**, 2371 (1986).
[12] J. D. Anderson and S. M. Grimes, Phys. Rev. C **41**, 2904 (1990).
[13] R. S. Gowda, S. S. V. Suryanarayana, and S. Ganesan, arXiv:nucl-th/0506004v1.
[14] A. M. Lane, Nucl. Phys. **35**, 676 (1962).
[15] G. R. Satchler, *Direct Nuclear Reactions*, Int. Series of Monographs on Physics, Vol. 471 (Oxford University Press, Oxford, UK, 1983).
[16] F. S. Dietrich, J. D. Anderson, R. W. Bauer, and S. M. Grimes, Phys. Rev. C **68**, 064608 (2003).

[17] R. Capote *et al.*, Nucl. Data Sheets **110**, 3107 (2009).
[18] I. Angeli and J. Csikai, Nucl. Phys. A **170**, 577 (1971).
[19] R. W. Finlay, W. P. Abfalterer, G. Fink, E. Montei, T. Adami, P. W. Lisowski, G. L. Morgan, and R. C. Haight, Phys. Rev. C **47**, 237 (1993).
[20] W. P. Abfalterer, F. B. Bateman, F. S. Dietrich, R. W. Finlay, R. C. Haight, and G. L. Morgan, Phys. Rev. C **63**, 044608 (2001).
[21] F. S. Dietrich *et al.*, Phys. Rev. C **67**, 044606 (2003).
[22] W. T. Diamond, Nucl. Instrum. Methods A **432**, 471 (1999).
[23] S. Essabaa *et al.*, Nucl. Instrum. Methods B **204**, 780 (2003).
[24] W. Hauser and H. Feshbach, Phys. Rev. **87**, 366 (1952).
[25] Projection angular momentum -coupled evaporation code (PACE2).
[26] Tapan Mukhopadhyay and D. N. Basu, Phys. Rev. C **76**, 064610 (2007).
[27] Tapan Mukhopadhyay and D. N. Basu, Phys. Rev. C **79**, 017602 (2009).